AGU PUBLICATIONS

Water Resources Research

RESEARCH ARTICLE

10.1002/2017WR021290

Key Points:

- Precipitation IDF curves can significantly underestimate flood risk or lead to unnecessary cost in regions that have significant snowpack
- Snowmelt and rain-on-snow events need to be specifically incorporated in analyses of extreme events in snow-dominated regions
- Next-generation IDF curves can overcome the deficiency of traditional precipitation-based IDF and enhance infrastructure resilience

Supporting Information:

- Supporting Information S1

Correspondence to:
M. Wigmosta,
mark.wigmosta@pnnl.gov

Citation:
Yan, H., Sun, N., Wigmosta, M., Skaggs, R., Hou, Z., & Leung, R. (2018). Next-generation intensity-duration-frequency curves for hydrologic design in snow-dominated environments. *Water Resources Research*, *54*, 1093–1108. https://doi.org/10.1002/2017WR021290

Received 9 JUN 2017
Accepted 28 JAN 2018
Accepted article online 1 FEB 2018
Published online 21 FEB 2018

Next-Generation Intensity-Duration-Frequency Curves for Hydrologic Design in Snow-Dominated Environments

Hongxiang Yan[1], Ning Sun[1], Mark Wigmosta[1,2], Richard Skaggs[1], Zhangshuan Hou[1], and Ruby Leung[3]

[1]Energy and Environment Directorate, Pacific Northwest National Laboratory, Richland, Washington, United States, [2]Distinguished Faculty Fellow, Department of Civil and Environmental Engineering, University of Washington, Seattle, Washington, United States, [3]Earth and Biological Sciences Directorate, Pacific Northwest National Laboratory, Richland, Washington, United States

Abstract There is a renewed focus on the design of infrastructure resilient to extreme hydrometeorological events. While precipitation-based intensity-duration-frequency (IDF) curves are commonly used as part of infrastructure design, a large percentage of peak runoff events in snow-dominated regions are caused by snowmelt, particularly during rain-on-snow (ROS) events. In these regions, precipitation-based IDF curves may lead to substantial overestimation/underestimation of design basis events and subsequent overdesign/underdesign of infrastructure. To overcome this deficiency, we proposed next-generation IDF (NG-IDF) curves, which characterize the actual water reaching the land surface. We compared NG-IDF curves to standard precipitation-based IDF curves for estimates of extreme events at 376 Snowpack Telemetry (SNOTEL) stations across the western United States that each had at least 30 years of high-quality records. We found standard precipitation-based IDF curves at 45% of the stations were subject to underdesign, many with significant underestimation of 100 year extreme events, for which the precipitation-based IDF curves can underestimate water potentially available for runoff by as much as 125% due to snowmelt and ROS events. The regions with the greatest potential for underdesign were in the Pacific Northwest, the Sierra Nevada Mountains, and the Middle and Southern Rockies. We also found the potential for overdesign at 20% of the stations, primarily in the Middle Rockies and Arizona mountains. These results demonstrate the need to consider snow processes in the development of IDF curves, and they suggest use of the more robust NG-IDF curves for hydrologic design in snow-dominated environments.

Plain Language Summary Recent natural disasters highlight the need for proper hydrologic design of infrastructure to accommodate extreme flood events. Hydraulic structures such as flood drainage systems are typically designed to convey a storm of a given duration and frequency of occurrence (e.g., the 100 year, 24 h storm event). These events are characterized by curves of a given frequency showing the relationship between precipitation intensity and duration (i.e., IDF curves). In locations with significant snowfall, standard precipitation-based IDF curves fail to capture the snowmelt and rain-on-snow events which may lead to substantial overestimation/underestimation of design basis events used for infrastructure. This study proposed next-generation IDF (NG-IDF) curves to overcome this deficiency. We used observed daily precipitation and changes in snow water equivalent at 376 Snowpack Telemetry (SNOTEL) stations to construct and compare standard precipitation and NG-IDF curves for estimates of extreme events across the western United States. Standard precipitation-based IDF curves were subject to underdesign at 45% of the stations in the Pacific Northwest, the Sierra Nevada Mountains, and the Middle and Southern Rockies. Underestimation of 100 year, 24 h events can be as much as 125%. These results suggest use of the more robust NG-IDF curves for hydrologic design in snow-dominated environments.

1. Introduction

Intensity-duration-frequency (IDF) curves are a worldwide standard tool used in planning and hydrologic design of infrastructure and water facilities to accommodate extreme hydrometeorological events (Chow, 1964). Traditionally, IDF curves are constructed using meteorological records of rainfall or precipitation data based on the common consensus that extreme rainfall events are more intense than snowmelt events (Cheng & AghaKouchak, 2014; Fassnacht & Records, 2015; Perica et al., 2013; Sarhadi & Soulis, 2017). In the United States, IDF curves are typically constructed based on the precipitation-frequency atlas referred to as Atlas 14 and produced by the National Oceanic and Atmospheric Administration (NOAA) (Perica et al., 2013). The IDF curves are then used to derive design storms of specified precipitation frequency and duration for use in event-based hydrologic rainfall-runoff models, such as the Natural Resources Conservation Service TR-55 (Cronshey et al., 1986) and U.S. Army Corps of Engineers Hydrologic Engineering Center Hydrologic Modeling System (HEC-HMS) models (Scharffenberg & Fleming, 2010).

Traditional IDF-based hydrologic design implicitly assumes precipitation is in the form of rainfall that is immediately subject to "rainfall-runoff" processes. This assumption has potentially significant implications in regions, where snowfall is a major component of precipitation. In these regions, precipitation-based IDF curves may lead to substantial overestimation or underestimation of design basis events and subsequent overdesign/underdesign of infrastructure. If an extreme precipitation event is primarily snowfall, much of the precipitation may not be immediately available for the rainfall-to-runoff process, which can lead to overdesign and incur unnecessary cost. On the other hand, underdesign will occur if snowmelt or rain-on-snow (ROS) rates exceed extreme precipitation, potentially leading to significant underestimates of flood risk.

In the hydrologic science community, the deficiency of traditional precipitation-based IDF design in snow-dominated environments is addressed by using physically based hydrologic models to simulate streamflow directly, instead of relying on the precipitation-based IDF curve to drive an event-based hydrologic model (Gudmundsson et al., 2012; Lee et al., 2016; Leung & Wigmosta, 1999; Mote et al., 2005; Tohver et al., 2014). These physically based hydrologic models, such as the Variable Infiltration Capacity (VIC) (Liang et al., 1994), the Distributed Hydrology Soil Vegetation Model (DHSVM) (Wigmosta et al., 1994), the Precipitation Runoff Modeling System (PRMS) (Leavesley et al., 1983), the Weather Research and Forecasting Model Hydrological modeling extension package (WRF-Hydro) (Gochis et al., 2015), and the Council for Regulatory Environmental Modeling (CREM) (EPA, 2009), use an energy-balance and mass-balance approach to track both snow accumulation and melt, as well as soil moisture and runoff generation. Other stand-alone snow models, such as the SNOW-17 (Anderson, 1976), the iSnobal (Marks et al., 1999), and the Utah Energy Balance (UEB) Snow Model (Tarboton et al., 1995), are also available and widely used in research (Hay & Clark, 2003; Painter et al., 2016; Raleigh & Lundquist, 2012).

However, a large portion of infrastructure in snow-dominated regions is currently designed using traditional IDF technology, including the NOAA precipitation-based IDF curves. It is common and standard practice for engineers to use a single-event-based model (e.g., TR-55) for modeling the rainfall-runoff process. The use of an advanced physically based modeling approach can be cost-prohibitive in the design of smaller infrastructure, such as residential storm water systems or highway culverts. Another important constraint is adherence to local surface water design manuals. These design manuals may recommend or require use of precipitation-based IDF curves with selected single-event hydrologic models. For example, the Federal Unified Facilities Criteria (UFC) recommend the Natural Resources Conservation Service (NRCS) TR-55 approach to modeling the rainfall-runoff process in surface drainage design (UFC, 2013). Snohomish County in Washington State extends from the Puget Sound lowland to the crest of the Cascade Mountains and watersheds range from rain-dominant, to transitional rain-snow, and to snow-dominant. However, the county drainage manual recommends the NOAA precipitation-based IDF curves combined with the NRCS curve number approach in infrastructure design of facilities such as wetpool treatment facilities (https://snohomishcountywa.gov/DocumentCenter/View/31221). In some cases, local regulations recommend adjustments to precipitation-based IDF curves. Chelan County, Washington, which contains snow-dominant watersheds on the eastern slope of the Cascade Mountains, follows the Stormwater Management Manual for Eastern Washington (https://fortress.wa.gov/ecy/publications/documents/0410076.pdf), which provides a method for adjusting precipitation-based IDF values to account for ROS events. This approach is provided for nine locations and assumes the observed December–February average daily snow depth will melt during a 72 h ROS event. Reductions are made to estimate melt for a 24 h time period, which is then added to the 24 h design storm precipitation estimate for that location.

In these locations, tradition IDF-based design is being applied with little knowledge of potential errors or opportunities for improvement. Therefore, the use of observational data to estimate potential errors in IDF-based hydrologic design is of great value when evaluating the adequacy of existing infrastructure and current infrastructure design using traditional approaches. This paper provides such an analysis and suggests a potential improvement through the use of next-generation IDF curves based on observation alone or in combination with physically based model simulations of hydrologic processes that control water delivery to the land surface.

IDF curve technology was first introduced in hydrology more than 50 years ago, generally for application in ungauged basins. Since then, the use of physically based hydrologic models for understanding hydrologic processes and predicting hydrologic responses has become more common. However, due to the high cost of the advanced physically based models (i.e., staff expertise, labor, and computational demand) and local regulation as discussed above, it can be expected that the IDF-based technology will continue to play a significant role in hydrologic design through the foreseeable future, especially for the design of small-scale infrastructure. Adaptations of the current IDF technology, rather than a complete technological change to a physically based hydrologic modeling approach, is also more likely to be implemented by agencies and regulators. Given the lack of consistency in how the IDF design approach is applied in regions that feature important snow processes, the goals of this study are to:

1. Investigate the role of snow processes in the amount of water available at the land surface for runoff during extreme events.
2. Identify the potential errors associated with the use of precipitation-based IDF curves in snow-dominated regions.
3. Introduce the next-generation IDF (NG-IDF) curves that account for snow processes and quantify the amount of water reaching the land surface for improved hydrologic design in snow-dominated environments. These curves are based on the water available for runoff (W) at the land surface acquired through rainfall, snowmelt, or ROS events.

It is important to note that the NG-IDF curves developed in this study have applications beyond hydrologic design. They illustrate relative differences between extreme rainfall and extreme snowmelt, which is important for analyses of hydrologic effects of climate change (Adam et al., 2009; Harpold & Kohler, 2017; Musselman et al., 2017). They also illustrate the spatial patterns, frequency, and magnitude of large ROS events throughout the western United States. In addition, NG-IDF curves can be used to examine climate stationarity outside the context of hydrologic modeling, as even the most sophisticated hydrologic models cannot replace the observation record (Milly et al., 2008).

This paper is organized as follows: section 2 describes the study area and discusses the importance of snow processes in the western United States. Section 3 describes the data source and quality control process. Section 4 presents the methodology for developing the NG-IDF curves, followed by the results and discussion of the NG-IDF curves in section 5. Finally, section 6 concludes the paper.

2. Study Area: Western United States

In the western United States, most annual precipitation falls in winter or early spring, and much of it is temporarily stored as snowpack in high-altitude mountainous regions. Snowmelt from mountain snowpack contributes about 70–80% of the total annual runoff in the western United States (Bales et al., 2006; Clark et al., 2001; Fassnacht et al., 2003). Although extreme precipitation over a short time period is often the cause of extreme flood events, a great number of large flood events are associated with snowmelt from deep snowpack especially during ROS events (may also include flow through of liquid water due to drainage, i.e., snowpack can function as a porous medium during ROS events) (Bookhagen & Burbank, 2010; Fang et al., 2014; Kattelmann, 1997).

Waylen and Woo (1982) reported that large floods occurred because of either spring snowmelt or heavy winter rainfall in the Cascade Range of the Pacific Northwest (PNW). Jarrett (1990) and Kampf and Lefsky (2016) found that the magnitude of extreme rainfall events decreased significantly and peak flows were dominated by snowmelt at high altitudes in the Colorado Front Range. England et al. (2010) also indicated that the dominant flood-generating mechanism transitioned from rainfall in lower elevations to snowmelt in higher elevations. Fassnacht and Records (2015) compared the magnitudes of precipitation, rainfall, and snowmelt for the 24 h, 10 and 100 year return period events in Colorado. They emphasized that snowmelt was on average 15% and 8.9% greater than precipitation for the 10 and 100 year events, respectively. Further, Berghuijs et al. (2016) explored the dominant flood-generating mechanisms across the continental

United States and found that snowmelt and ROS events were more robust predictors of the flooding response than rainfall over the western United States.

ROS events, typically combined with warmer temperature and high winds, lead to significantly accelerated melting and produce severe flood events both in the mountainous regions and lowlands, often resulting in severe social and economic damage (Harr, 1981; Kattelmann, 1991; McCabe et al., 2007; Pradhanang et al., 2013; Sui & Koehler, 2001). The four highest floods on record in the Merced River in Yosemite National Park were all caused by ROS events (Kattelmann, 1997); the ROS event on February 1996 resulted in one of the largest floods in the PNW and millions dollars of damage (Marks et al., 1998).

3. Data Sources and Quality Control

We acquired long-term meteorological and snowpack measurements (through 30 September 2016) from 785 active Snowpack Telemetry (SNOTEL) stations across the western United States operated by the U.S. Department of Agriculture NRCS. In this data set, both snow water equivalent (*SWE*) and accumulated precipitation (*PREC*) values are reset to zero on 1 October at the start of each water year. The temporal resolution of more recent SNOTEL sensors is hourly. However, due to wind effect and sensor issues, the hourly data are less reliable than the daily data (Meyer et al., 2012). As a result, we used the daily (24 h) time series of SNOTEL records, including *PREC*, *SWE*, and air temperature values.

A three-stage filter was implemented on the raw SNOTEL data sets to address data quality concerns. The first and second stages of the filter follow the data quality control procedure described in detail by Serreze et al. (1999) to identify missing data, erroneous values, and outliers in *PREC*, air temperature, and *SWE* values. We also included an additional check on *SWE* values during the melt phase to make sure large changes in *SWE* are consistent with corresponding changes in air temperature values (described in the supporting information). We developed an additional third stage to address inconsistent *SWE* and *PREC* observations, where the *SWE* amount exceeds *PREC* amount throughout the snow season (physically impossible). The reader is referred to the supporting information for step-by-step descriptions of the first-stage and second-stage filters. The description below focuses on the third-stage filter.

The third-stage filter identifies “inconsistent water years,” which are defined according to Meyer et al. (2012) as when the maximum *SWE* value is at least 5% greater than the associated *PREC*. When an inconsistent water year was identified, data for the entire water year were removed from the station record. In addition, SNOTEL stations were excluded if the mean relative difference between the maximum *SWE* amount and the associated *PREC* amount taken over all inconsistent water years exceeded 20%. Although SNOTEL *SWE* data have been used in a great number of applications, very few attempts have been made to address the inconsistency issue (Johnson & Marks, 2004; Meyer et al., 2012). This is mainly due to the very complex sources that could be attributed to such inconsistency, e.g., precipitation undercatch and snowpack overcatch (i.e., snow drifting, ice-bridging, and foreign material deposition). Investigation of the exact responsible mechanism for the SNOTEL inconsistency is beyond the scope of this work. Nevertheless, the effects of the inconsistent data on IDF curve design are further discussed in the supporting information.

4. Methods

4.1. Estimation of Precipitation, Rainfall, and Water Available for Runoff

The actual amount of the water (W) reaching land surface available for the runoff process is characterized through mass balance as $W = P - \Delta SWE$, where the 24 h precipitation (P) is directly calculated as the difference between the current and previous daily *PREC*. To explore the viability of traditional IDF curves, we generated annual maximum time series from daily values for total precipitation, rainfall only, and W for four hydrometeorological conditions (classes 3–6 below):

1. Total precipitation (P): as measured at the SNOTEL site,
2. Rainfall only (R): precipitation with no snowfall,
3. W from melt without precipitation (M_o): no precipitation with a decrease in *SWE*,
4. W from melt associated with mixed rainfall and snowfall (M_mix): *PREC* increase larger than *SWE* increase,
5. W from all melt events including ROS events (M_ros): decrease in *SWE* with or without precipitation, and
6. W from all events (W_all), i.e., all melt events (M_ros) plus rainfall on snow-free ground.

10.1002/2017WR021290

Table 1
Rainfall/Snowmelt Classification Based on the Daily SNOTEL Accumulated Precipitation (PREC) and Snow Water Equivalent (SWE) Data Sets

Class	24 h intensity	Classification method
2	Rainfall only: *R*	if $\Delta SWE = 0$: $R = \Delta PREC$
3	Melt without precipitation: *M_o*	if ($\Delta SWE < 0$) and ($\Delta PREC = 0$): $M\_o = -\Delta SWE$
4	Mixed rain/snowfall/melt: *M_mix*	if ($\Delta SWE > 0$) and ($\Delta PREC > 0$) and ($\Delta PREC > \Delta SWE$): $M\_mix = \Delta PREC - \Delta SWE$
5	All melt events including ROS events: *M_ros*	if $\Delta SWE < 0$: $M\_ros = \Delta PREC - \Delta SWE$

The NG-IDF curves are developed based only on *W_all*; classes 2–5 are used to quantify the relative role of melt/rainfall/ROS in contributing to extreme runoff. Classification for classes 2–5 are provided in Table 1.

Our approach uses the change in *SWE* instead of air temperature threshold to differentiate between rainfall and snowfall; limitations of the air temperature approach are discussed by McCabe et al. (2007) and Fassnacht and Records (2015). For example, the precipitation phase in NOAA Atlas 14 (Perica et al., 2013) was determined based on an assumed 1.1°C temperature threshold. However, many studies have demonstrated that a single temperature threshold is questionable because of the great variability of temperature thresholds both in space and time (Fassnacht, 2013; López-Moreno et al., 2013; Lundquist et al., 2008). Other atmospheric processes are also important controls on the precipitation phases, leading to a large temperature range in which precipitation falls as snow (Dai, 2008; Rajagopal & Harpold, 2016). Note our approach assumes that loss of *SWE* through sublimation has minor effects on the extreme events. During ROS events, the rate of sublimation is likely to be low due to higher humidity, but it could be larger on dry windy days.

4.2. IDF Curve Development

IDF curves were developed for SNOTEL stations that passed the three-stage filter and that each had at least 30 years of records for frequency analysis (Kuczera, 1982; Perica et al., 2013; Yan & Moradkhani, 2015). As noted above, we constructed six time series consisting of the annual maximum for *P*, *R*, *M_mix*, *M_o*, *M_ros*, and all viable events *W_all* (*M_ros* plus rainfall on snow-free ground) at each SNOTEL station. Frequency analysis methods used in IDF curve design are based on the underlying stationary assumption, which is that the hydroclimatic system fluctuates within an unchanging envelope of variability (Khaliq et al., 2006; Milly et al., 2008; Rosenberg et al., 2010). However, this stationary assumption is being challenged because of anthropogenic changes (Leung & Wigmosta, 1999; Sun et al., 2015, 2016; Taylor et al., 2012; Yan & Edwards, 2013). In this study, we tested the stationary assumption for the annual maximum series using the nonparametric Mann-Kendall test (Kendall, 1975; Mann, 1945) at the 5% significance level. Where trends were significant, we detrended the time series using Sen's slope (Sen, 1968) while maintaining the time series average. All trend analyses were performed using the "trend" package (Pohlert, 2016) in R (version 3.3.2).

After detrending, goodness-of-fit tests based on L-moments for three-parameter distributions were performed as suggested by Hosking and Wallis (1997) and Perica et al. (2013). All L-moments analyses performed in this study used the "lmom" and "lmomRFA" packages (Hosking, 2015a, 2015b) in R (version 3.3.2). Five three-parameter distributions were considered: the generalized logistic (GLO), generalized extreme value (GEV), generalized normal (GNO), Pearson type III (PE3), and generalized Pareto (GPA) distributions. The IDF curves were then designed based on the best fit distribution for five exceedance probabilities: 1/5, 1/10, 1/25, 1/50, and 1/100, which correspond to the extreme events with return periods of 5, 10, 25, 50, and 100 years.

4.3. Assessment of NG-IDF Curves in Engineering Design

By comparing the NG-IDF with the traditional precipitation-based IDF curve values, we evaluated the potential design risk for a given duration and frequency, as follows (Figure 1):

1. overdesign—if the precipitation IDF value is greater than the NG-IDF value (Figure 1a);
2. underdesign—if the NG-IDF value is greater than the precipitation IDF value (Figure 1b); and
3. proper design—if the differences between the precipitation IDF and NG-IDF values are less than 10% (Figure 1c).

10.1002/2017WR021290

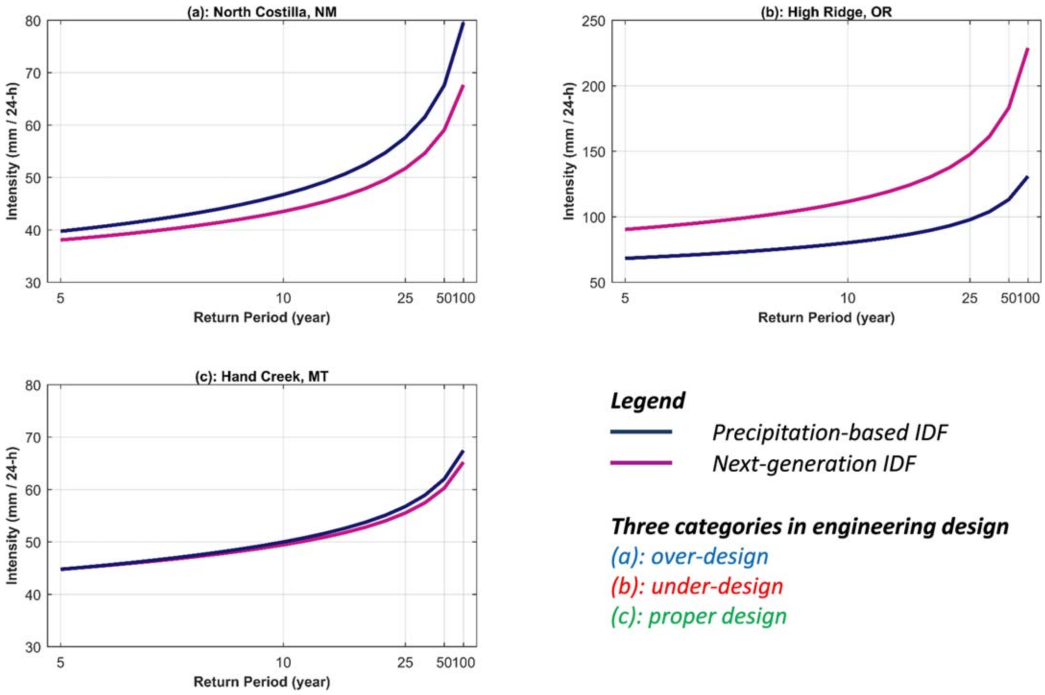

Figure 1. The 24 h precipitation-based and next-generation intensity-duration-frequency (NG-IDF) curves for the three design classes. (a) Overdesign when the precipitation IDF value is greater than the NG-IDF value. (b) Underdesign when the NG-IDF value is greater than the precipitation IDF value. (c) Proper design when the differences between the precipitation IDF and NG-IDF values are less than 10%.

We used a 10% relative difference as the tolerance threshold for proper design to account for data uncertainty in frequency analysis. We acknowledge that this value is somewhat arbitrary and could be higher (more discussion follows in section 5.3).

5. Results and Discussions

5.1. Data Screening

SNOTEL data were screened according to the three-stage filter described in section 3. The first two stages removed a total of 0.2%, 0.4%, and 1.7% of the observations for *PREC*, *SWE*, and air temperature values, respectively. The third-stage filter excluded 43 SNOTEL stations and removed about 10% of the total station data (from the remaining stations) associated with inconsistent water years. The three-stage filtering process retained a total of 376 stations each of which had at least 30 years of records (Figure 2a) out of 785 active SNOTEL stations. About half of the retained stations had at least 35 years of records. Qualitatively, the selected SNOTEL stations show good spatial coverage over the western United States (i.e., the Cascade Range, Blue Mountains, Sierra Nevada, Rocky Mountains, and Arizona/New Mexico).

Figures 2b and 2c show the total number of inconsistent water years and the mean relative differences between the peak *SWE* value and the associated *PREC* value for each retained station. It should be noted that there were very few inconsistent water years identified for stations in the Cascade Range as well as lower elevation regions. Stations in the Sierra Nevada, Rocky Mountains, and higher elevation regions, however, had larger amounts of inconsistent data. Similar findings were reported by Meyer et al. (2012). As noted previously, all inconsistent water year data were removed.

5.2. Spatial Variability of Snowpack

Many studies have documented the accumulation and melt of snowpack in the western United States (Clow, 2010; Knowles et al., 2006; McCabe & Clark, 2005; Mote, 2006; Musselman et al., 2017; Payne et al.,

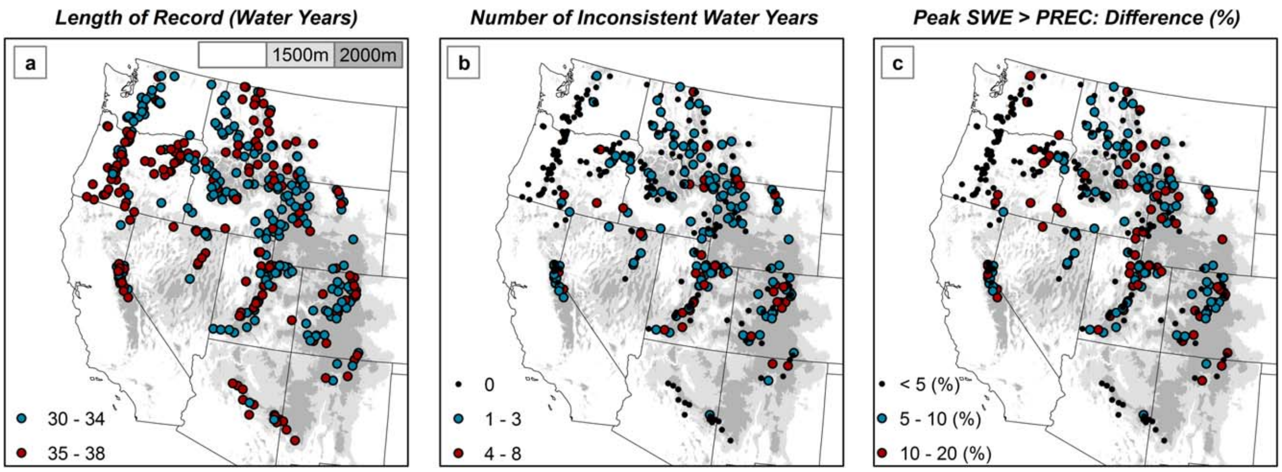

Figure 2. (a) The length of record in water years (without the inconsistent data) of the screened 376 SNOTEL stations in the western United States. (b) The total number of inconsistent water years for each SNOTEL station (defined as: peak *SWE* value at least 5% higher than the corresponding *PREC* value). (c) The mean percentage difference between each SNOTEL station's peak *SWE* and associated *PREC* (as the reference) values over all the inconsistent water years. Unless noted, all inconsistent water years were removed from the analysis.

2004; Regonda et al., 2005; Serreze et al., 1999, 2001). Although our primary focus was the development of IDF curves, we also examined the spatial variability in the magnitude and timing of peak *SWE* values.

Figure 3a presents the mean peak *SWE* values for all selected SNOTEL stations. The highest mean peak *SWE* values (greater than 918 mm) were found in the PNW, Sierra Nevada, and northern Rockies in Idaho and Montana. The higher peak *SWE* values in the PNW and Sierra Nevada are expected as a result of their overall wetter conditions in winter. The high peak *SWE* value for the northern Rockies is mainly due to the frequent leeside cyclogenesis and occasional passage of Pacific systems (Cayan, 1996; Whittaker & Horn, 1984). The lower peak *SWE* values (less than 358 mm) in the Colorado Front Range, Blue Mountains, and Arizona/New Mexico are associated with limited precipitation (Serreze et al., 1999). Figure 3b shows the average date of the climatological peak *SWE* value. The earliest peak *SWE* value date (in February) occurs in Arizona/New Mexico, mainly because of the comparatively higher winter temperature. The dates of peak *SWE* values in the PNW and Sierra Nevada occur in late March to early April. Most stations in the interior regions, including the Colorado Front Range, Wasatch Mountains, and Rocky Mountains in Idaho and Wyoming, showed the

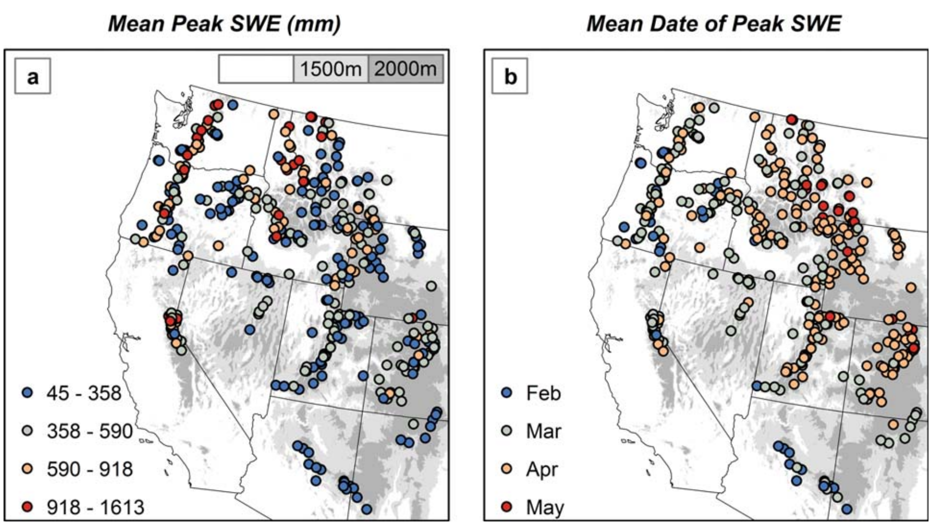

Figure 3. (a) The mean annual peak *SWE* value in mm for each SNOTEL station over the total length of record. (b) The mean date of the annual peak *SWE* value.

latest dates of peak *SWE* value in April to early May, which is related to the later onset of above-freezing temperatures (Serreze et al., 2001).

5.3. Precipitation-Rain-Snowmelt Frequency Analysis

For each SNOTEL station, we examined trends in the 24 h annual maximum series using the Mann-Kendall test. There were statistically significant negative trends in annual maximum 24 h *P*, *R*, *M_mix*, *M_o*, *M_ros*, and *W_all* at 4.0%, 6.1%, 18.6%, 30.6%, 21.3%, and 16.2% of the 376 selected stations, respectively. Trends were small and ranged from −5.1 to −2.3 mm per decade for *P*, −5.1 to −1.5 mm per decade for *R*, −10.9 to −0.8 mm per decade for *M_mix*, −15.2 to −2.2 mm per decade for *M_o*, −16.4 to −2.3 mm per decade for *M_ros*, and −15.8 to −2.3 mm per decade for *W_all*. Fewer SNOTEL stations showed positive trends: 2.1%, 1.6%, 0.5%, 0.8%, 0.8%, and 1.1% of all stations for *P*, *R*, *M_mix*, *M_o*, *M_ros*, and *W_all*, respectively. We detrended the annual maximum series for stations that had statistically significant trends using Sen's slope while maintaining the time series average. Summary of the trend analysis results are provided in Table 2.

As noted previously, we evaluated five three-parameter distributions to describe the annual data (after detrending). Based on the Z^{DIST} value simulation method proposed by Hosking and Wallis (1997), the GLO provided the best fit across all SNOTEL stations for all six annual maximum series. We used this distribution (GLO) in all frequency analysis for the following three reasons. First, changes in distribution type for different annual maximum series often result in considerable discontinuities in frequency estimation across series, particularly at large return periods (Hosking & Wallis, 1997; Perica et al., 2013). Second, the actual form of the frequency analysis distribution is unknown and its derivation from the physical processes is still a fundamental unsolved problem in hydrology (Griffis & Stedinger, 2007; Lima & Lall, 2010; Yan & Moradkhani, 2015). Third, the uncertainty in the frequency analysis associated with the types of distribution is generally small. Many studies have suggested that the major uncertainty in frequency analysis is contributed by the data themselves, while the choice of distribution plays a much less important role (Fassnacht & Records, 2015; Hosking & Wallis, 1997; Stedinger & Griffis, 2008; Yan & Moradkhani, 2016b).

Detrending had little effect on the frequency analysis. For instance, among the 83 SNOTEL stations with statistically significant *M_ros* trends, the original *M_ros* annual maximum data set exceeded the detrended values by −1.5%–8.3% for the 10 year and −6.5%–37.9% for the 100 year events. Based on the predefined 10% difference threshold of proper design, the differences between the original and detrended values were smaller than the threshold at all 83 stations for 10 year events and 51 stations for 100 year events. Averaged among all 83 stations, the original *M_ros* were 2% and 8% higher than the detrended values for the 10 and 100 year events, which were smaller than the 10% threshold. The Pearson correlation coefficients between original and detrended values were greater than 0.98 for both the 10 and 100 year *M_ros* events. The other five annual maximum data sets showed similar results.

In the case of the mixed rain/snow/melt (*M_mix*), the annual peak values were much smaller than the all melt events including the ROS case (*M_ros*) at most of the SNOTEL stations. For instance, the 10 and 100 year *M_ros* events were greater than *M_mix* at 99.7% and 93.9% of all stations, respectively. Averaged over the 376 stations, the *M_ros* 10 and 100 year events were 31.6 and 38.6 mm more than the *M_mix* events,

Table 2
Summary of Trend Analysis Results for the Six Annual Maximum Data Sets

	24 h annual maximum data set					
	P	*R*	*M_mix*	*M_o*	*M_ros*	*W_all*
Significant negative trends						
Stations (%)	4.0	6.1	18.6	30.6	21.3	16.2
Trend range (mm/decade)	[−5.1, −2.3]	[−5.1, −1.5]	[−10.9, −0.8]	[−15.2, −2.2]	[−16.4, −2.3]	[−15.8, −2.3]
Significant positive trends						
Stations (%)	2.1	1.6	0.5	0.8	0.8	1.1
Trend range (mm/decade)	[3.2, 6.4]	[3.5, 11.0]	[2.1, 7.3]	[3.6, 5.6]	[4.2, 9.1]	[2.7, 9.7]

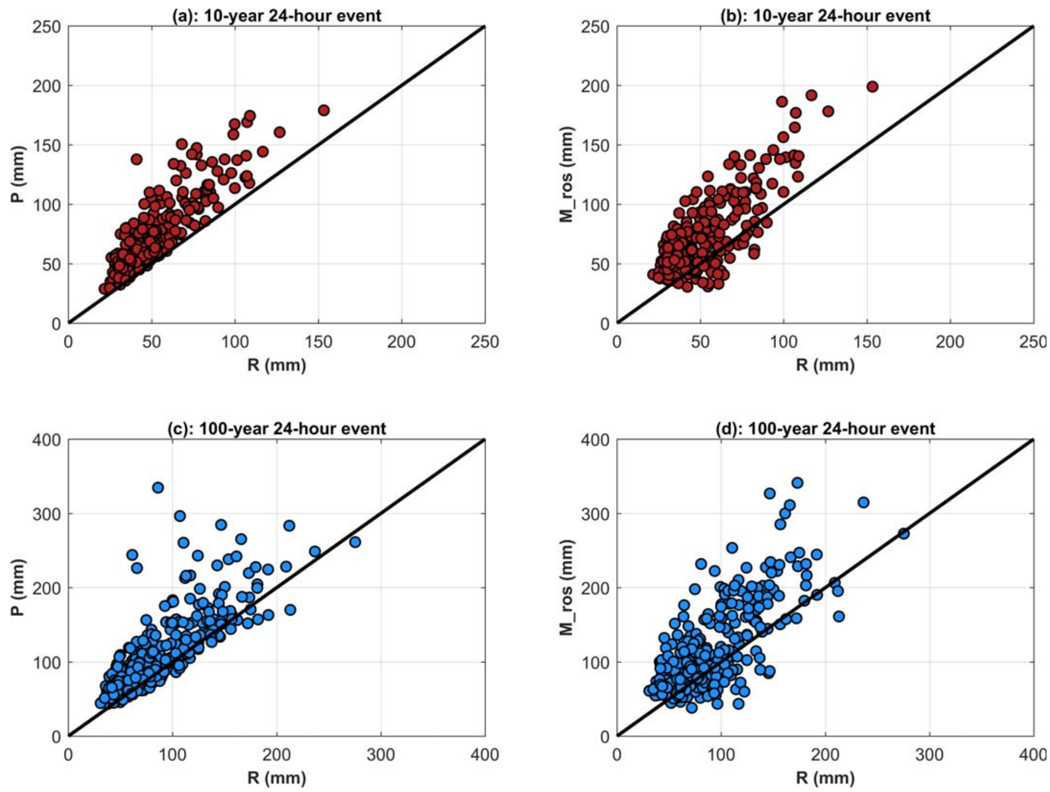

Figure 4. The 10 and 100 year, 24 h precipitation (*P*), rainfall only (*R*), and all melt events, including rain-on-snow events (*M_ros*) for the 376 SNOTEL stations across the western United States. The black line indicates the 1:1 line. Note that for some stations, the 100 year 24 h rainfall events are larger in magnitude than precipitation; this physical impossibility has been reported in previous studies and is due to data uncertainty and the statistical nature of frequency analysis (more specifically, overextension with high uncertainty due to small sample size).

respectively. As a result, the mixed/rain/snow/melt *M_mix* had little effect on the IDF analysis that characterizes the potential extremes, and is not considered in the following discussion.

Figure 4 compares the 10 and 100 year, 24 h precipitation (*P*) versus rainfall only (*R*) and all melt events including ROS events (*M_ros*) versus rainfall only (*R*) for the 376 SNOTEL stations. On average, the 10 and 100 year *P* was 26% greater (ranging from 2.4% to 70.3%) and 17% greater (−25.3 to 74.8%) than the corresponding *R*, respectively. As expected, these results indicate that the majority of the extreme precipitation events in the snow-dominated regions of the western United States had significant snowfall. We found that the maximum annual precipitation series for all stations contained at least one event caused by snowfall, while an average of 69% of the data in the annual maximum precipitation series over all stations contained snowfall. The 10 year *P* events were greater than *R* events at all stations. It should be noted that 63 of the 376 stations showed greater *R* events than *P* events for the 100 year event (Figure 4c). This physical impossibility has been reported in previous studies and is due to data uncertainty (e.g., precipitation gauge undercatch) and the statistical nature of frequency analysis (more specifically, overextension with high uncertainty due to small sample size) (Fassnacht & Records, 2015; Haan, 2002; Perica et al., 2013). In this study, we used a difference threshold 10% as proper design class to partially capture this uncertainty. Averaged among all 63 stations, the *R* 100 year events were 7% higher than the *P* events, which was smaller than the 10% threshold. The 10 and 100 year, 24 h all melt events including ROS (*M_ros*) were greater than the corresponding rainfall only (*R*) by more than 10% at 311 and 237 out of the 376 stations (Figures 4b, 4d, 5a, and 5c). Among these stations, the *M_ros* exceeded *R* by 3–84 mm for the 10 year event and by 5–174 mm for the 100 year event. Rainfall *R* exceeded *M_ros* by more than 10% at 20 and 65 stations, respectively, corresponding to the exceedances of 5–27 mm for the 10 year event and 6–71 mm for the 100 year event. Averaged over all stations, the 10 and 100 year *M_ros* was 43% greater and 30% greater, respectively, than the corresponding *R*.

10.1002/2017WR021290

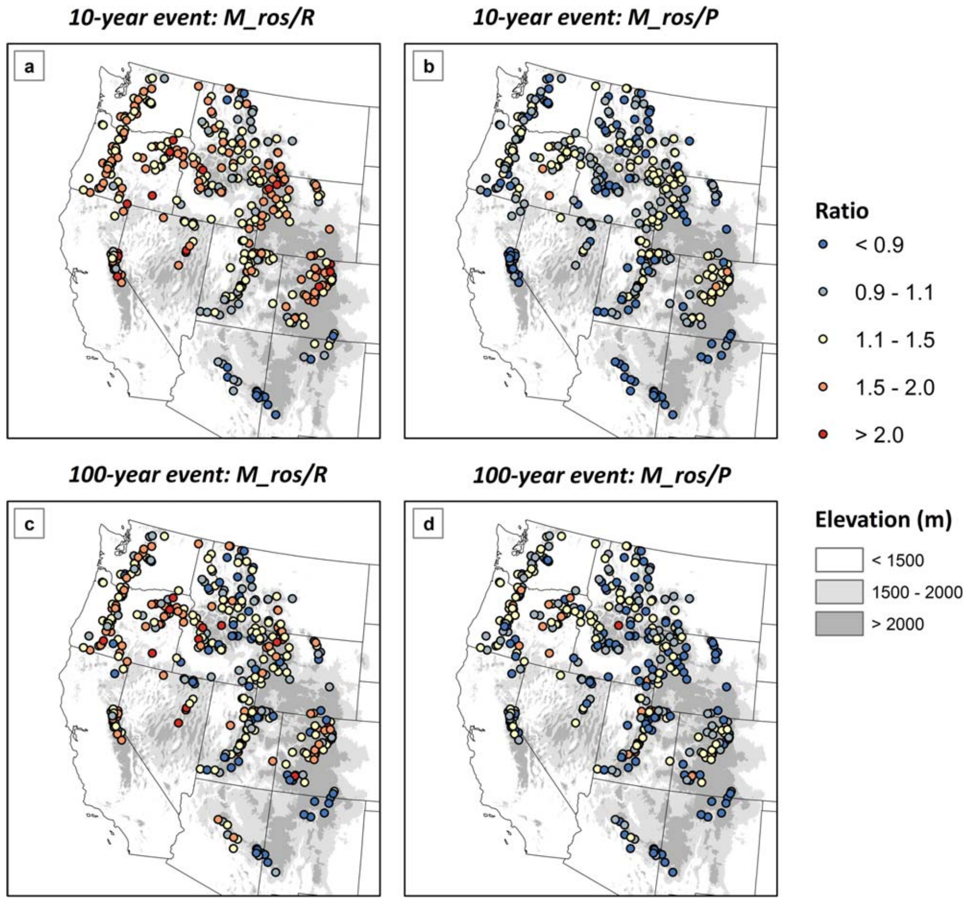

Figure 5. Ratio of the 10 and 100 year, 24 h all melt events including rain-on-snow (*M_ros*) to the precipitation (*P*) and rainfall only (*R*) for the 376 SNOTEL stations across the western United States. Ratios less than 1.0 indicate *M_ros* events smaller than *P* or *R*; while ratios greater than 1.0 suggest *M_ros* events exceed *P* or *R*.

Figure 5 shows the ratios between the 10 and 100 year, 24 h all melt events including ROS (*M_ros*) versus precipitation (*P*) and rainfall only (*R*) for the 376 SNOTEL stations. As expected, *M_ros* was greater than the corresponding *R* at more stations and by a larger ratio than *P* at the same stations. The *M_ros* exceeded *P* by more than 10% at 127 and 142 out of the 376 stations for the 10 and 100 year events, respectively. For these stations, the M_ros/P ratios range from 1.1 to 1.8 and from 1.1 to 2.2 for the 10 and 100 year events. Larger M_ros/P ratios were observed in the Cascade Range, Colorado Front Range, Blue Mountains, and northern Rockies. The largest ratio occurred at the Idarado station in Colorado; it had a value of 2.2 for the 100 year event. In general, these results illustrate the deficiency of the traditional precipitation-based IDF curves and emphasize the role of snowmelt events in providing water available for runoff in mountainous environments.

5.4. Importance of Rain-on-Snow Events for IDF Design

To better understand the influence of ROS events on NG-IDF curves, we compared snowmelt IDF curves developed with ROS (*M_ros*) and without ROS (*M_o*) (Table 1). Figure 6a shows the percentage of ROS events in the total annual maximum *M_ros* data set for the 376 SNOTEL stations. The figure shows that ROS events were more frequent in the PNW, where most of the stations in the Cascade Range had more than 70% ROS events in the annual maximum series. The ROS events were much less frequent (<20%) in the Colorado Front Range and Wasatch Range. Similar findings were also reported by McCabe et al. (2007) based on the analyses of cooperative weather station data in the western United States.

Figures 6b and 6c present the ratios between *M_ros* and *M_o* for the 10 and 100 year events, respectively. The ratio M_ros/M_o was greater than 1.1 at 197 and 303 out of the 376 stations, respectively. The largest

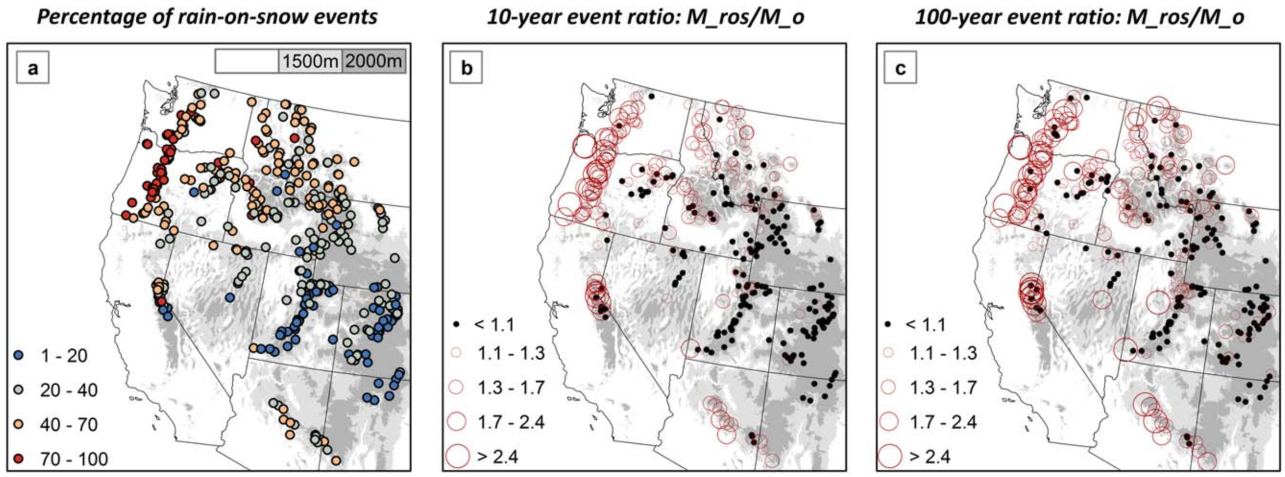

Figure 6. (a) The percentage of rain-on-snow events (decrease in *SWE* value accompanied by precipitation) in the total annual maximum *M_ros* data set for the 376 stations. (b) The 10 year, 24 h events ratio between all melt events including rain-on-snow (*M_ros*) and melt without precipitation (*M_o*) as described in Table 1. (c) Similar to (b) but showing the ratio for the 100 year, 24 h events. Note that the rain-on-snow events substantially increase both 10 and 100 year events across the western United States and lead to potentially higher flood risk.

difference occurred at the Seine Creek station in Oregon, where the ratio of M_ros/M_o was 4.9 for the 100 year event. On average, when ROS events were included, the 10 and 100 year events increased by 26% and 35%, respectively. These results suggest that snowmelt without precipitation (*M_o*) IDF curves can substantially underestimate extreme events in some locations (especially in the PNW and Sierra Nevada), and further emphasize the importance of including ROS events to generate more robust NG-IDF curves.

5.5. NG-IDF in Hydrologic Design

After demonstrating the importance of snowmelt and ROS events in IDF design in the previous two sections, the main focus of this section is to assess the traditional precipitation-based IDF in hydrologic design using NG-IDF curves, which characterize the actual water (*W_all*) reaching the land surface. As described in section 4.3, we evaluated the potential design risk in three classes: overdesign, underdesign, and proper design.

The relative differences between the NG-IDF and precipitation-based IDF curves for the 10 and 100 year events are presented in Figure 7 for all SNOTEL stations. About 45% and 43% of the 376 stations indicated the potential for underdesign for the 24 h, 10 and 100 year events, respectively. For these stations, *W_all* exceeded *P* by 10–75% for the 10 year event and 10–125% for the 100 year event. The largest difference (125%) occurred at the Idarado station in Colorado. The potential for overdesign exists at 9% and 20% of the 376 stations, corresponding to negative relative differences between *W_all* and *P* of -34 to -10% for the 10 year event and -75 to -10% for the 100 year event, respectively. A total of 137 stations were shown to be properly designed (*P* and *W_all* within $\pm10\%$) for both 10 and 100 year events. Most of the stations found to be underdesigned were in the PNW, Colorado Front Range, and Wasatch Mountains. In general, these regions are characterized by deeper snowpack and longer snow accumulation seasons, as shown in Figure 3.

The West Coast showed higher spatial coherence in underdesign and overdesign classes than the interior mountains, because this region is the first to intercept pulses of Pacific moisture. Serreze et al. (2001) also noted that the SNOTEL stations in the western United States tended to have a few large individual snowfall events and that large snowfall at a given station was not necessarily observed at surrounding stations in Colorado, Wyoming, and Utah, due to strong localized topographic controls. It is interesting to note that a few stations in the Sierra Nevada Mountains showed overdesign of the 10 year event but underdesign of the 100 year event. We found that the NG-IDF and precipitation-based IDF curves at these stations crossed, leading to the contradictory design class for 10 and 100 year events. In the Sierra Nevada Mountains, most extreme precipitation falling during the winter is associated with large atmospheric river landfalls. As a

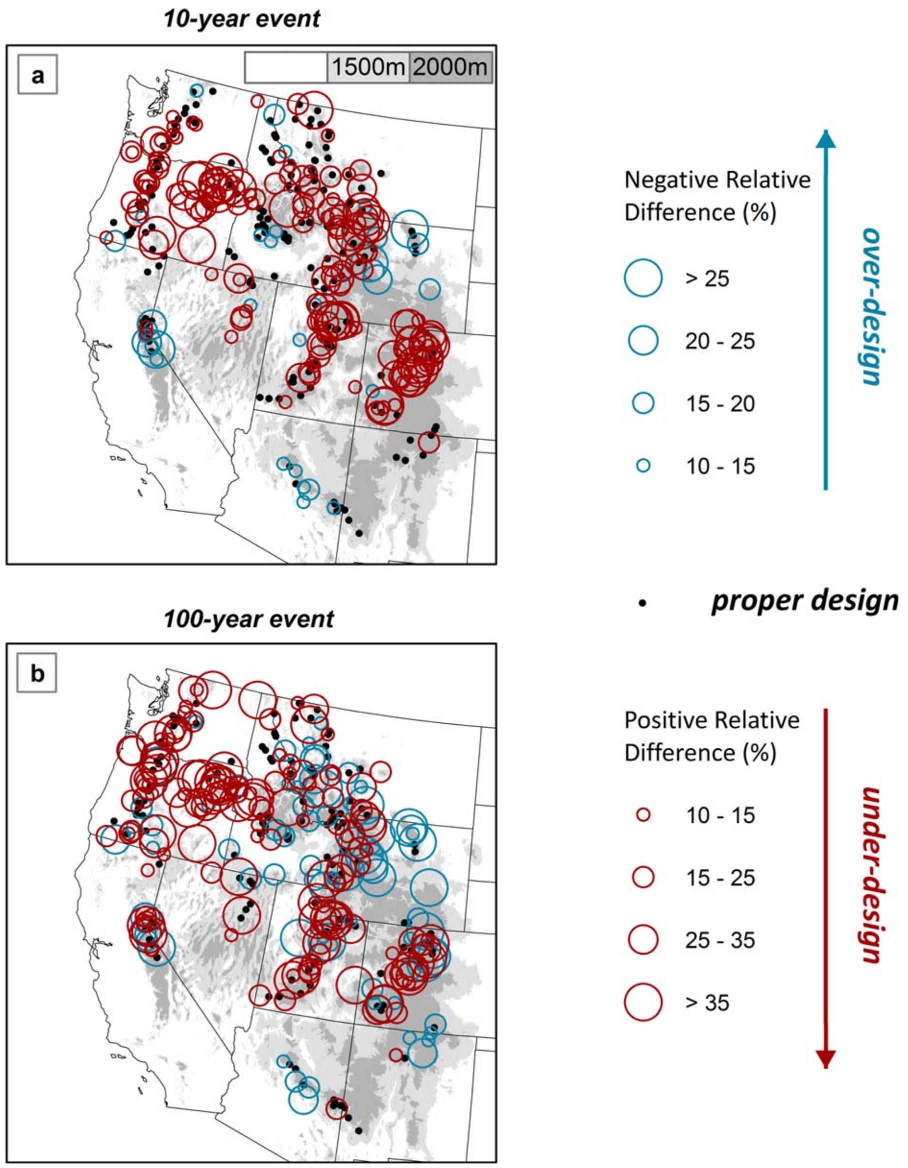

Figure 7. Relative percentage of differences ($(W\_all-P)/P\times100$) of the 10 and 100 year, 24 h events between actual water available for runoff (W_all) from the NG-IDF and precipitation (P) from the traditional IDF curves. Stations with red circles indicate underdesign ($W\_all > P$); stations with blue circles suggest overdesign ($P > W\_all$); and black dots indicate proper design for the stations. The diameter of the circles indicates the magnitude of the relative difference.

result, annual maximum series were dominated by precipitation (P) rather than melt events. However, when a higher *SWE* value than average occurs due to atmospheric variability (Clark et al., 1999; Clark & Serreze, 2000), the accelerated melt of deep snowpack combined with rainfall during ROS events produce a significantly higher amount of available water than generated by peak precipitation alone (Kattelmann, 1991). As a result, the ROS events tend to dominate the 100 year event estimators and induce some of the worst flooding events in this region, e.g., the 1983 Sierra Nevada flood.

In summary, the 100 year NG-IDF value was 40% higher than the 100 year precipitation-based IDF value at 35 of the 376 SNOTEL stations, while the converse (P was 40% higher than W_all) was observed at only 12 stations (Figure 8). On average, the magnitudes of W_all were 24% and 30% greater than P across all the underdesigned stations in the western United States for the 10 and 100 year events, respectively; while, the magnitudes of P were on average 19% and 31% greater than W_all across all the overdesigned stations for the 10 and 100 year events, respectively. These results emphasize the potential flood risk or unnecessary

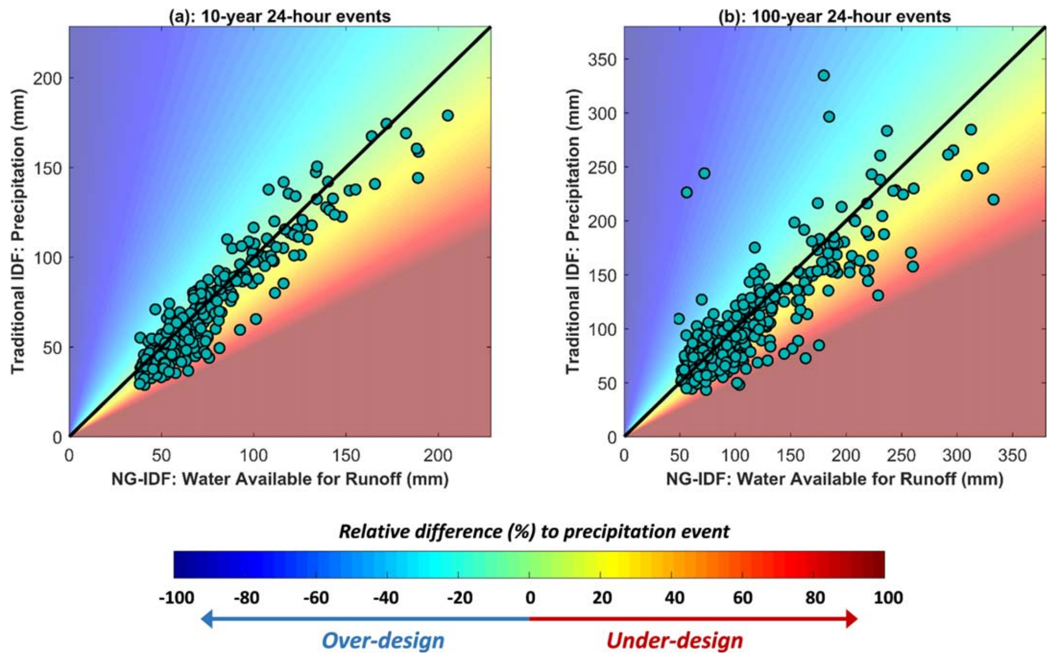

Figure 8. Scatterplots of 10 and 100 year, 24 h precipitation *P* (traditional IDF) versus actual water available for runoff (*W_all* used in NG-IDF) events for the 376 SNOTEL stations across the western United States. The black line indicates the 1:1 line; warmer color represents the underdesign of an infrastructure; and colder color suggests the overdesign of an infrastructure.

cost associated with snowmelt and ROS events and the importance of incorporating NG-IDF curves in engineering design.

6. Conclusions

In this study, we first examined the role of snowmelt and rain-on-snow (ROS) events in analyses of extreme runoff events for 376 SNOTEL stations across the western United States. Our results suggest that the majority of extreme precipitation events in the snow-dominated regions of the western United States were snowfall and that melt with ROS can significantly exceed extreme precipitation events. More specifically, all melt events including ROS exceeded precipitation by more than 10% at 127 and 142 out of the 376 stations for the 10 and 100 year, 24 h events; the associated ratios ranged from 1.1 to 1.8 and from 1.1 to 2.2, respectively. This brings into question the reliability and resilience of infrastructure design in snow-dominated regions using the standard precipitation-based IDF curves, as recommended in many local surface water design manuals.

To overcome the deficiency of the IDF technology in snow-dominated environments, we proposed the next-generation IDF (NG-IDF) curves, which characterize the actual water reaching land surface (*W_all*) through a mass-balance approach to improve infrastructure design in these regions. Through comparison to precipitation-based IDF curves, we found about 45% of the stations in the western United States showed the potential for underdesign, mainly in Pacific Northwest, the Sierra Nevada, and the Middle and Southern Rockies, meaning that the precipitation-based IDF curves may substantially underestimate water available for runoff generation. Conversely, about 20% of the stations show the potential for overdesign, primarily in the Middle Rockies and Arizona mountains.

We acknowledge and fully support the use of physically based hydrologic modeling as an alternative approach to accounting for the snow effect on extreme runoff that is largely ignored in the precipitation-based IDF design in snow-dominated regions. This approach, however, suffers from lack of guidance in local regulations and corresponding surface water design manuals, high-computational and labor costs to implement, and its own limitations such as parameter and model structure uncertainties (Clark et al., 2015; Sun et al., 2014; Yan & Moradkhani, 2016a). It can be expected that IDF-based technology will continue to play a significant role in hydrologic design in the foreseeable future, especially for small-scale infrastructure design. Consequently, the proposed NG-IDF curves would benefit resources engineering and design in snow-dominated regions. While this study focused on the western United States, the proposed NG-IDF can have a broader impact on resilient infrastructure in snow-dominated regions (i.e., mountains and valleys) worldwide.

A limitation of this study is the relatively coarse spatial and temporal coverage of the SNOTEL-based NG-IDF curves. Due to the daily step of SNOTEL data, we developed NG-IDF curves (24 h duration) at 376 stations across the western United States. We acknowledge that these 376 NG-IDF curves would not provide full spatial coverage for practical hydrologic design purposes. A practical path forward that we are currently implementing is to use a physically based hydrologic model (DHSVM) driven by high-resolution gridded metrological data to estimate *W_all* in finer spatial detail across the western United States. The resulting NG-IDF curves then can be extended from the coastal lowlands to high-elevation snowmelt-dominated basins. Other duration curves, from 1 to 12 h, can also be developed in a similar fashion. In addition, the NG-IDF curves based on observations developed here also provide an important new validation data set for these more comprehensive modeling efforts.

Acknowledgments
All daily SNOTEL data used in this study are available from the Natural Resources Conservation Service and National Water and Climate Center at <https://www.wcc.nrcs.usda.gov/snow/> (last access 9 February 2017). The Digital Elevation Model data were obtained from the United States Geological Survey and the National Geospatial-Intelligence Agency Global Multi-resolution Terrain Elevation Data 2010 data set at <https://lta.cr.usgs.gov/GMTED2010> (last access 17 February 2017). The United States boundaries shown in the figures were acquired from United States Geological Survey Small-scale Data set State Boundaries of the United States 200506 Shapefile at <https://catalog.data.gov/dataset/usgs-small-scale-dataset-state-boundaries-of-the-united-states-200506-shapefile> (last access 17 February 2017). This material is based upon work supported by the Strategic Environmental Research and Development Program under contract RC-2546. Battelle Memorial Institute operates the Pacific Northwest National Laboratory (PNNL) for the U.S. Department of Energy under contract DE-AC06–76RLO-1830. The QA/QC screened SNOTEL observations at the 785 stations used in this paper will be available at the PNNL website: https://dhsvm.pnnl.gov/. We thank Dr. Alan Hamlet and two anonymous reviewers whose comments and suggestions during the review process substantially improved the paper.

References

Adam, J. C., Hamlet, A. F., & Lettenmaier, D. P. (2009). Implications of global climate change for snowmelt hydrology in the twenty-first century. *Hydrological Processes*, *23*(7), 962–972. https://doi.org/10.1002/hyp.7201

Anderson, E. A. (1976). *A point energy and mass balance model of a snow cover* (NOAA Tech. Rep. NWS 19, 150 pp.). Silver Spring, MD: National Oceanic and Atmospheric Administration.

Bales, R. C., Molotch, N. P., Painter, T. H., Dettinger, M. D., Rice, R., & Dozier, J. (2006). Mountain hydrology of the western United States. *Water Resources Research*, *42*, W08432. https://doi.org/10.1029/2005WR004387

Berghuijs, W. R., Woods, R. A., Hutton, C. J., & Sivapalan, M. (2016). Dominant flood generating mechanisms across the United States. *Geophysical Research Letters*, *43*, 4382–4390. https://doi.org/10.1002/2016GL068070

Bookhagen, B., & Burbank, D. W. (2010). Toward a complete Himalayan hydrological budget: Spatiotemporal distribution of snowmelt and rainfall and their impact on river discharge. *Journal of Geophysical Research: Earth Surface*, *115*, F03019. https://doi.org/10.1029/2009JF001426

Cayan, D. R. (1996). Interannual climate variability and snowpack in the Western United States. *Journal of Climate*, *9*(5), 928–948. https://doi.org/10.1175/1520-0442(1996)009 < 0928:ICVASI>2.0.CO;2

Cheng, L., & AghaKouchak, A. (2014). Nonstationary precipitation intensity-duration-frequency curves for infrastructure design in a changing climate. *Scientific Reports*, *4*, 7093. https://doi.org/10.1038/srep07093

Chow, V. T. (1964). *Handbook of applied hydrology: A compendium of water-resources technology*. New York, NY: McGraw-Hill.

Clark, M. P., Nijssen, B., Lundquist, J. D., Kavetski, D., Rupp, D. E., Woods, R. A., et al. (2015). A unified approach for process-based hydrologic modeling: 1. Modeling concept. *Water Resources Research*, *51*, 2498–2514. https://doi.org/10.1002/2015WR017198

Clark, M. P., & Serreze, M. C. (2000). Effects of variations in East Asian snow cover on modulating atmospheric circulation over the North Pacific Ocean. *Journal of Climate*, *13*(20), 3700–3710. https://doi.org/10.1175/1520-0442(2000)013<3700:EOVIEA>2.0.CO;2

Clark, M. P., Serreze, M. C., & McCabe, G. J. (2001). Historical effects of El Nino and La Nina events on the seasonal evolution of the montane snowpack in the Columbia and Colorado River Basins. *Water Resources Research*, *37*(3), 741–757. https://doi.org/10.1029/2000WR900305

Clark, M. P., Serreze, M. C., & Robinson, D. A. (1999). Atmospheric controls on Eurasian snow extent. *International Journal of Climatology*, *19*(1), 27–40. https://doi.org/10.1002/(SICI)1097-0088(199901)19:1<27::AID-JOC346>3.0.CO;2-N

Clow, D. W. (2010). Changes in the timing of snowmelt and streamflow in Colorado: A response to recent warming. *Journal of Climate*, *23*(9), 2293–2306. https://doi.org/10.1175/2009JCLI2951.1

Cronshey, R., McCuen, R. H., Miller, N., Rawls, W., Robbins, S., & Woodward, D. (1986). *Urban hydrology for small watersheds* (TR-55). Washington, DC: U.S. Department of Agriculture (USDA).

Dai, A. (2008). Temperature and pressure dependence of the rain-snow phase transition over land and ocean. *Geophysical Research Letters*, *35*, L12802. https://doi.org/10.1029/2008GL033295

England, J. F., Godaire, J. E., Klinger, R. E., Bauer, T. R., & Julien, P. Y. (2010). Paleohydrologic bounds and extreme flood frequency of the Upper Arkansas River, Colorado, USA. *Geomorphology*, *124*(1–2), 1–16. https://doi.org/10.1016/j.geomorph.2010.07.021

EPA (2009). *Guidance on the development, evaluation, and application of environmental models, council for regulatory environmental modeling*. Washington, DC: U.S. Environmental Protection Agency.

Fang, S., Xu, L., Pei, H., Liu, Y., Liu, Z., Zhu, Y., et al. (2014). An integrated approach to snowmelt flood forecasting in water resource management. *IEEE Transactions on Industrial Informatics*, *10*(1), 548–558. https://doi.org/10.1109/TII.2013.2257807

Fassnacht, S. R. (2013). The probability of precipitation as snow derived from daily air temperature for high elevation areas of Colorado, United States. In *Cold and mountain region hydrological systems under climate change: Towards improved projections* (pp. 65–70). Gothenburg, Sweden: IAHS.

Fassnacht, S. R., Dressler, K. A., & Bales, R. C. (2003). Snow water equivalent interpolation for the Colorado River Basin from snow telemetry (SNOTEL) data. *Water Resources Research*, *39*(8), 1208. https://doi.org/10.1029/2002WR001512

Fassnacht, S. R., & Records, R. M. (2015). Large snowmelt versus rainfall events in the mountains. *Journal of Geophysical Research: Atmospheres*, *120*, 2375–2381. https://doi.org/10.1002/2014JD022753

Gochis, D. J., Yu, W., & Yates, D. N. (2015). *The NCAR WRF-hydro technical description and user's guide version 3.0* (NCAR Technical Document, 120 p.). Boulder, CO: National Center for Atmospheric Research. Retrieved from http://www.ral.ucar.edu/projects/wrf_hydro/

Griffis, V. W., & Stedinger, J. R. (2007). Log-Pearson Type 3 distribution and its application in flood frequency analysis. II: Parameter estimation methods. *Journal of Hydrologic Engineering*, *12*(5), 492–500. https://doi.org/10.1061/(ASCE)1084-0699(2007)12:5(492)

Gudmundsson, L., Wagener, T., Tallaksen, L. M., & Engeland, K. (2012). Evaluation of nine large-scale hydrological models with respect to the seasonal runoff climatology in Europe. *Water Resources Research*, *48*, W11504. https://doi.org/10.1029/2011WR010911

Haan, C. T. (2002). *Statistical methods in hydrology* (2nd ed.). Hoboken, NJ: Wiley-Blackwell.

Harpold, A. A., & Kohler, M. (2017). Potential for changing extreme snowmelt and rainfall events in the mountains of the Western United States. *Journal of Geophysical Research: Atmospheres*, *122*, 13219–13228. https://doi.org/10.1002/2017JD027704

Harr, R. D. (1981). Some characteristics and consequences of snowmelt during rainfall in western Oregon. *Journal of Hydrology*, *53*(3–4), 277–304. https://doi.org/10.1016/0022-1694(81)90006-8

Hay, L. E., & Clark, M. P. (2003). Use of statistically and dynamically downscaled atmospheric model output for hydrologic simulations in three mountainous basins in the western United States. *Journal of Hydrology*, *282*(1–4), 56–75. https://doi.org/10.1016/S0022-1694(03)00252-X

Hosking, J. R. M. (2015a). *Package "lmom"*. Retrieved from https://www.r-project.org/

Hosking, J. R. M. (2015b). *Package "lmomRFA"*. Retrieved from https://www.r-project.org/

Hosking, J. R. M., & Wallis, J. R. (1997). *Regional frequency analysis: An approach based on L-moments*. Cambridge, UK: Cambridge University Press.

Jarrett, R. D. (1990). Paleohydrologic techniques used to define the spatial occurrence of floods. *Geomorphology*, *3*(2), 181–195. https://doi.org/10.1016/0169-555X(90)90044-Q

Johnson, J. B., & Marks, D. (2004). The detection and correction of snow water equivalent pressure sensor errors. *Hydrological Processes*, *18*(18), 3513–3525. https://doi.org/10.1002/hyp.5795

Kampf, S. K., & Lefsky, M. A. (2016). Transition of dominant peak flow source from snowmelt to rainfall along the Colorado Front Range: Historical patterns, trends, and lessons from the 2013 Colorado Front Range floods. *Water Resources Research*, *52*, 407–422. https://doi.org/10.1002/2015WR017784

Kattelmann, R. (1991). Peak flows from snowmelt runoff in the Sierra Nevada, USA. In H. Bergmann et al. (Eds.), *Snow, hydrology and forests in high alpine areas, Proceedings of the Vienna Symposium*, August 1991 (IAHS Publ. 205, pp. 203–211). Wallingford, UK: IASH Publication.

Kattelmann, R. (1997). Flooding from rain-on-snow events in the Sierra Nevada. In G. H. Leavesley et al. (Eds.), *Destructive water: Water-caused natural disasters, their abatement and control*, *Proceedings of the Conference held at Anaheim*, California, June 1996 (IAHS, pp. 59–65). Wallingford, UK: IASH Publication.

Kendall, M. G. (1975). *Rank correlation methods*. London: Griffin.

Khaliq, M. N., Ouarda, T. B. M. J., Ondo, J.-C., Gachon, P., & Bobée, B. (2006). Frequency analysis of a sequence of dependent and/or non-stationary hydro-meteorological observations: A review. *Journal of Hydrology*, *329*(3–4), 534–552. https://doi.org/10.1016/j.jhydrol.2006.03.004

Knowles, N., Dettinger, M. D., & Cayan, D. R. (2006). Trends in snowfall versus rainfall in the Western United States. *Journal of Climate*, *19*(18), 4545–4559. https://doi.org/10.1175/JCLI3850.1

Kuczera, G. (1982). Robust flood frequency models. *Water Resources Research*, *18*(2), 315–324. https://doi.org/10.1029/WR018i002p00315

Leavesley, G. H., Lichty, R. W., Thoutman, B. M., & Saindon, L. G. (1983). *Precipitation-runoff modeling system: User's manual*. Colorado, CO: US Geological Survey.

Lee, S.-Y., Hamlet, A. F., & Grossman, E. E. (2016). Impacts of climate change on regulated streamflow, hydrologic extremes, hydropower production, and sediment discharge in the Skagit River Basin. *Northwest Science*, *90*(1), 23–43. https://doi.org/10.3955/046.090.0104

Leung, L. R., & Wigmosta, M. S. (1999). Potential climate change impacts on mountain watersheds in the Pacific Northwest. *Journal of the American Water Resources Association*, *35*(6), 1463–1471. https://doi.org/10.1111/j.1752-1688.1999.tb04230.x

Liang, X., Lettenmaier, D. P., Wood, E. F., & Burges, S. J. (1994). A simple hydrologically based model of land surface water and energy fluxes for general circulation models. *Journal of Geophysical Research: Atmospheres*, *99*(D7), 14415–14428. https://doi.org/10.1029/94JD00483

Lima, C. H. R., & Lall, U. (2010). Spatial scaling in a changing climate: A hierarchical Bayesian model for non-stationary multi-site annual maximum and monthly streamflow. *Journal of Hydrology*, *383*, 307–318. https://doi.org/10.1016/j.jhydrol.2009.12.045

López-Moreno, J. I., Fassnacht, S. R., Heath, J. T., Musselman, K. N., Revuelto, J., Latron, J., et al. (2013). Small scale spatial variability of snow density and depth over complex alpine terrain: Implications for estimating snow water equivalent. *Advances in Water Resources*, *55*, 40–52. https://doi.org/10.1016/j.advwatres.2012.08.010

Lundquist, J. D., Neiman, P. J., Martner, B., White, A. B., Gottas, D. J., & Ralph, F. M. (2008). Rain versus snow in the Sierra Nevada, California: Comparing Doppler profiling radar and surface observations of melting level. *Journal of Hydrometeorology*, *9*(2), 194–211. https://doi.org/10.1175/2007JHM853.1

Mann, H. B. (1945). Nonparametric tests against trend. *Econometrica*, *13*(3), 245. https://doi.org/10.2307/1907187

Marks, D., Domingo, J., Susong, D., Link, T., & Garen, D. (1999). A spatially distributed energy balance snowmelt model for application in mountain basins. *Hydrological Processes*, *13*(12–13), 1935–1959. https://doi.org/10.1002/(SICI)1099-1085(199909)13:12/13<1935::AID-HYP868>3.0.CO;2-C

Marks, D., Kimball, J., Tingey, D., & Link, T. (1998). The sensitivity of snowmelt processes to climate conditions and forest cover during rain-on-snow: A case study of the 1996 Pacific Northwest flood. *Hydrological Processes*, *12*(10–11), 1569–1587. https://doi.org/10.1002/(SICI)1099-1085(199808/09)12:10/11<1569::AID-HYP682>3.0.CO;2-L

McCabe, G. J., & Clark, M. P. (2005). Trends and variability in snowmelt runoff in the Western United States. *Journal of Hydrometeorology*, *6*(4), 476–482. https://doi.org/10.1175/JHM428.1

McCabe, G. J., Hay, L. E., & Clark, M. P. (2007). Rain-on-snow events in the Western United States. *Bulletin of the American Meteorological Society*, *88*(3), 319–328. https://doi.org/10.1175/BAMS-88-3-319

Meyer, J. D. D., Jin, J., & Wang, S.-Y. (2012). Systematic patterns of the inconsistency between snow water equivalent and accumulated precipitation as reported by the snowpack telemetry network. *Journal of Hydrometeorology*, *13*(6), 1970–1976. https://doi.org/10.1175/JHM-D-12-066.1

Milly, P. C. D., Betancourt, J., Falkenmark, M., Hirsch, R. M., Kundzewicz, Z. W., Lettenmaier, D. P., et al. (2008). Stationarity is dead: Whither water management? *Science*, *319*(5863), 573–574. https://doi.org/10.1126/science.1151915

Mote, P. W. (2006). Climate-driven variability and trends in Mountain Snowpack in Western North America*. *Journal of Climate*, *19*(23), 6209–6220. https://doi.org/10.1175/JCLI3971.1

Mote, P. W., Hamlet, A. F., Clark, M. P., & Lettenmaier, D. P. (2005). Declining mountain snowpack in Western North America*. *Bulletin of the American Meteorological Society*, *86*(1), 39–49. https://doi.org/10.1175/BAMS-86-1-39

Musselman, K. N., Clark, M. P., Liu, C., Ikeda, K., & Rasmussen, R. (2017). Slower snowmelt in a warmer world. *Nature Climate Change*, *7*(3), 214–219. https://doi.org/10.1038/nclimate3225

Painter, T. H., Berisford, D. F., Boardman, J. W., Bormann, K. J., Deems, J. S., Gehrke, F., et al. (2016). The Airborne Snow Observatory: Fusion of scanning lidar, imaging spectrometer, and physically-based modeling for mapping snow water equivalent and snow albedo. *Remote Sensing of Environment*, *184*, 139–152. https://doi.org/10.1016/j.rse.2016.06.018

Payne, J. T., Wood, A. W., Hamlet, A. F., Palmer, R. N., & Lettenmaier, D. P. (2004). Mitigating the effects of climate change on the water resources of the Columbia River Basin. *Climatic Change*, *62*(1–3), 233–256. https://doi.org/10.1023/B:CLIM.0000013694.18154.d6

Perica, S., Martin, D., Pavlovic, S., Roy, I., Laurent, M., St. Trypaluk, C., et al. (2013). *Precipitation-frequency atlas of the United States* (NOAA Atlas 14, Vol. 8, version 2.0). Silver Spring, MD: U.S. Department of Commerce, National Oceanic and Atmospheric Administration, National Weather Service.

Pohlert, T. (2016). *Package "trend"*. Retrieved from https://www.r-project.org/

Pradhanang, S. M., Frei, A., Zion, M., Schneiderman, E. M., Steenhuis, T. S., & Pierson, D. (2013). Rain-on-snow runoff events in New York. *Hydrological Processes*, *27*(21), 3035–3049. https://doi.org/10.1002/hyp.9864

Rajagopal, S., & Harpold, A. A. (2016). Testing and improving temperature thresholds for snow and rain prediction in the Western United States. *Journal of the American Water Resources Association*, *52*(5), 1142–1154. https://doi.org/10.1111/1752-1688.12443

Raleigh, M. S., & Lundquist, J. D. (2012). Comparing and combining SWE estimates from the SNOW-17 model using PRISM and SWE reconstruction. *Water Resources Research*, *48*, W01506. https://doi.org/10.1029/2011WR010542

Regonda, S. K., Rajagopalan, B., Clark, M., & Pitlick, J. (2005). Seasonal cycle shifts in hydroclimatology over the Western United States. *Journal of Climate*, *18*(2), 372–384. https://doi.org/10.1175/JCLI-3272.1

Rosenberg, E. A., Keys, P. W., Booth, D. B., Hartley, D., Burkey, J., Steinemann, A. C., et al. (2010). Precipitation extremes and the impacts of climate change on stormwater infrastructure in Washington State. *Climatic Change*, *102*(1–2), 319–349. https://doi.org/10.1007/s10584-010-9847-0

Sarhadi, A., & Soulis, E. D. (2017). Time-varying extreme rainfall intensity-duration-frequency curves in a changing climate. *Geophysical Research Letters*, *44*, 2454–2463. https://doi.org/10.1002/2016GL072201

Scharffenberg, W. A., & Fleming, M. J. (2010). *Hydrologic modeling system HEC-HMS: User's manual*. Davis, CA: U.S. Army Corps of Engineers Hydrological Engineering Center (HEC).

Sen, P. K. (1968). Estimates of the regression coefficient based on Kendall's Tau. *Journal of the American Statistical Association*, *63*(324), 1379–1389. https://doi.org/10.1080/01621459.1968.10480934

Serreze, M. C., Clark, M. P., Armstrong, R. L., McGinnis, D. A., & Pulwarty, R. S. (1999). Characteristics of the western United States snowpack from snowpack telemetry (SNOTEL) data. *Water Resources Research*, *35*(7), 2145–2160. https://doi.org/10.1029/1999WR900090

Serreze, M. C., Clark, M. P., & Frei, A. (2001). Characteristics of large snowfall events in the montane western United States as examined using snowpack telemetry (SNOTEL) data. *Water Resources Research*, *37*(3), 675–688. https://doi.org/10.1029/2000WR900307

Stedinger, J. R., & Griffis, V. W. (2008). Flood frequency analysis in the United States: Time to update. *Journal of Hydrologic Engineering*, *13*(4), 199–204. https://doi.org/10.1061/(ASCE)1084-0699(2008)13:4(199)

Sui, J., & Koehler, G. (2001). Rain-on-snow induced flood events in Southern Germany. *Journal of Hydrology*, *252*(1–4), 205–220. https://doi.org/10.1016/S0022-1694(01)00460-7

Sun, N., Hong, B., & Hall, M. (2014). Assessment of the SWMM model uncertainties within the generalized likelihood uncertainty estimation (GLUE) framework for a high-resolution urban sewershed. *Hydrological Processes*, *28*(6), 3018–3034. https://doi.org/10.1002/hyp.9869

Sun, N., Yearsley, J., Baptiste, M., Cao, Q., Lettenmaier, D. P., & Nijssen, B. (2016). A spatially distributed model for assessment of the effects of changing land use and climate on urban stream quality. *Hydrological Processes*, *30*(25), 4779–4798. https://doi.org/10.1002/hyp.10964

Sun, N., Yearsley, J., Voisin, N., & Lettenmaier, D. P. (2015). A spatially distributed model for the assessment of land use impacts on stream temperature in small urban watersheds. *Hydrological Processes*, *29*(10), 2331–2345. https://doi.org/10.1002/hyp.10363

Tarboton, D. G., Chowdhury, T. G., & Jackson, T. H. (1995). A spatially distributed energy balance snowmelt model. In K. A. Tonnessen, M. W. Williams, & M. Tranter (Eds.), *Biogeochemistry of seasonally snow-covered catchments* (IAHS Publ. 228, pp. 141–155). Wallingford, UK: IASH Publication.

Taylor, K. E., Stouffer, R. J., & Meehl, G. A. (2012). An overview of CMIP5 and the experiment design. *Bulletin of the American Meteorological Society*, *93*(4), 485–498. https://doi.org/10.1175/BAMS-D-11-00094.1

Tohver, I. M., Hamlet, A. F., & Lee, S.-Y. (2014). Impacts of 21st-century climate change on hydrologic extremes in the Pacific Northwest Region of North America. *Journal of the American Water Resources Association*, *50*(6), 1461–1476. https://doi.org/10.1111/jawr.12199

UFC (2013). *Surface drainage design* (150/5320-5D). Washington, DC: U.S. Department of Transportation, Federal Aviation Administration. Retrieved from https://www.faa.gov/documentLibrary/media/Advisory_Circular/150_5320_5d.pdf

Waylen, P., & Woo, M. (1982). Prediction of annual floods generated by mixed processes. *Water Resources Research*, *18*(4), 1283–1286. https://doi.org/10.1029/WR018i004p01283

Whittaker, L. M., & Horn, L. H. (1984). Northern Hemisphere extratropical cyclone activity for four mid-season months. *Journal of Climatology*, *4*(3), 297–310. https://doi.org/10.1002/joc.3370040307

Wigmosta, M. S., Vail, L. W., & Lettenmaier, D. P. (1994). A distributed hydrology-vegetation model for complex terrain. *Water Resources Research*, *30*(6), 1665–1679. https://doi.org/10.1029/94WR00436

Yan, H., & Edwards, F. G. (2013). Effects of land use change on hydrologic response at a watershed scale, Arkansas. *Journal of Hydrologic Engineering*, *18*(12), 1779–1785. https://doi.org/10.1061/(ASCE)HE.1943-5584.0000743

Yan, H., & Moradkhani, H. (2015). A regional Bayesian hierarchical model for flood frequency analysis. *Stochastic Environmental Research and Risk Assessment*, *29*(3), 1019–1036. https://doi.org/10.1007/s00477-014-0975-3

Yan, H., & Moradkhani, H. (2016a). Combined assimilation of streamflow and satellite soil moisture with the particle filter and geostatistical modeling. *Advances in Water Resources*, *94*, 364–378. https://doi.org/10.1016/j.advwatres.2016.06.002

Yan, H., & Moradkhani, H. (2016b). Toward more robust extreme flood prediction by Bayesian hierarchical and multimodeling. *Natural Hazards*, *81*(1), 203–225. https://doi.org/10.1007/s11069-015-2070-6